ARL-TR-10297 ● Mar 2026

Generating Bone-Like Internal Structure in Arbitrary 3-D Models

by Charles Epple, Aidan Fleischer, Ella Willetts, Sophia Knap, W. David Hairston, and Christopher G. Sinks

NOTICES

Disclaimers

ARL-TR-10297 ● MAR 2026

Generating Bone-Like Internal Structure in Arbitrary 3-D Models

Charles Epple, Aidan Fleischer, Ella Willetts, and Sophia Knap
Energetics Technology Center

W. David Hairston and Christopher G. Sinks
DEVCOM Army Research Laboratory

REPORT DOCUMENTATION PAGE

1. REPORT DATE	2. REPORT TYPE	3. DATES COVERED START DATE	3. DATES COVERED END DATE
March 2026	Technical Report	June 2024	September 2025

4. TITLE AND SUBTITLE
Generating Bone-Like Internal Structure in Arbitrary 3-D Models

5a. CONTRACT NUMBER	5b. GRANT NUMBER	5c. PROGRAM ELEMENT NUMBER
W911NF2530002		
5d. PROJECT NUMBER	**5e. TASK NUMBER**	**5f. WORK UNIT NUMBER**

6. AUTHOR(S)
Charles Epple, Aidan Fleischer, Ella Willetts, Sophia Knap, W. David Hairston, and Christopher G. Sinks

7. PERFORMING ORGANIZATION NAME(S) AND ADDRESS(ES)	8. PERFORMING ORGANIZATION REPORT NUMBER
DEVCOM Army Research Laboratory ATTN: FCDD-RLA-FC Aberdeen Proving Ground, MD 21005	ARL-TR-10297

9. SPONSORING/MONITORING AGENCY NAME(S) AND ADDRESS(ES)	10. SPONSOR/MONITOR'S ACRONYM(S)	11. SPONSOR/MONITOR'S REPORT NUMBER(S)

12. DISTRIBUTION/AVAILABILITY STATEMENT
DISTRIBUTION STATEMENT A. Approved for public release: distribution unlimited.

13. SUPPLEMENTARY NOTES
ORCIDs: Christopher G. Sinks, 0009-0003-5693-0274; W. David Hairston, 0000-0003-4432-8430; Sophia Knap, 0000-0002-3705-6070; Charles Epple 0009-0005-4560-6668; Aidan Fleischer 0009-0007-5141-4990

14. ABSTRACT
Operational environments continue to increase in complexity, increasing the breadth of Soldier exposure to novel risk. To understand and mitigate these risks, we require higher-complexity physical models. One area where current models fail to meet nascent requirements is correctly modeling trabecular bone. Here, we develop an algorithm to generate anatomically similar bone porosity toward these models. Through use of Blender software, we are able to create a Voroni matrix and apply it to arbitrary shapes with specific porosity gradients. We also calibrate the developed algorithm to account for errors encountered when 3-D printing these matrices, so the expected porosity aligns with the final part. Going forward, these models will allow us to create bone-like structures to examine physical and electromagnetic effects of battlefield conditions on tissue without putting Soldiers at risk.

15. SUBJECT TERMS
Humans in Complex Systems, Blender Modeling, Anatomical Modeling, Bone Structure, 3-D Printing, SLA Printing, Tissue Phantom, Tissue Surrogate, Porosity Generation

16. SECURITY CLASSIFICATION OF: a. REPORT	b. ABSTRACT	C. THIS PAGE	17. LIMITATION OF ABSTRACT	18. NUMBER OF PAGES
UNCLASSIFIED	UNCLASSIFIED	UNCLASSIFIED	UU	27

19a. NAME OF RESPONSIBLE PERSON	19b. PHONE NUMBER *(Include area code)*
Christopher G. Sinks	(520) 691-5358

STANDARD FORM 298 (REV. 5/2020)
Prescribed by ANSI Std. Z39.18

Contents

List of Figures

1. Introduction

Materials that mimic the physical properties of bone are commonly used for surgical trainers, traumatic brain injury research, ballistics testing, and medical device research.[1–3] However, current biomimetic materials do not sufficiently mimic biological structure or simultaneously capture mechanical and electromagnetic (EM) properties.[4] Soldiers increasingly operate around technology that emits different spectra of EM radiation, raising concerns about safety from long- or short-term exposure. We aim to create a material and structure that can mimic both the physical and EM properties of bone, allowing the simultaneous measurement of the effects of different forces upon the human body.

Bone structure generally consists of a dense outer cortical region, a porous inner cancellous region, other features like inner marrow in long bones, and a thin outer periosteum membrane. Dry bone is quite electrically resistive—with an admittance on the order of 1×10^{-6} mS/m.[5] However, the high water and salt content of live bone drastically changes both the mechanical bending modulus by 3 orders of magnitude[6] and admittance range to 15 mS/m.[7] To make an electrically biomimetic bone and decouple the tuning of mechanical and electrical properties, we plan to first recreate a structure similar to the porosity of live bone as reported in the literature[8] and then infuse it with a soft tissue-like gel at a later stage.

This report focuses on the creation of an arbitrary porous gradient in an arbitrary structure that can range from a simple cube to an extracted model of actual bone. We then print these models at high precision to calibrate and confirm the accuracy of our porosity generation.

2. Materials and Methods

2.1 Overview and Setup

Blender (v4.4, Blender Foundation; Amsterdam, the Netherlands) is a free, open-source 3-D creation software used widely for creating 3-D objects including still images, animations, video effects, and video editing.[9] Our interest lies in a specific aspect of Blender called “geometry nodes,” which allow for procedurally modeling and animating complex and dynamic objects.[9] This allows the application of arbitrary process algorithms to create complex models, like anatomical microstructure, reducing work time by orders of magnitude.

Our Blender geometry node algorithm for applying arbitrary bone-like porosity patterns to imported models is described in detail in Section 2.2. Sections 2.3 and

2.4 describe the printing process, and Section 2.5 describes model validation and confirmation.

2.2 Geometry Nodes Process

We started with a stereolithography file (.stl) of a 20- × 20- × 16-mm cube imported into Blender as a large file size and higher complexity can significantly increase workflow time. We have not identified a specific minimum thickness; however, anything less than the radius used in the porosity generation will struggle to produce printable geometry. From here, our node system can be applied to our cube (Figure 1).

Materials used in the production of porous structures are as follows.

1) Formlabs Form 4 SLA printer (Formlabs Inc.; Somerville, Massachusetts)
2) Formlabs Wash L
3) Formlabs Form Cure L
4) Formlabs PreForm 3.51.1.572
5) Formlabs Clear Resin V5 and Rigid 10K Resin V1.1

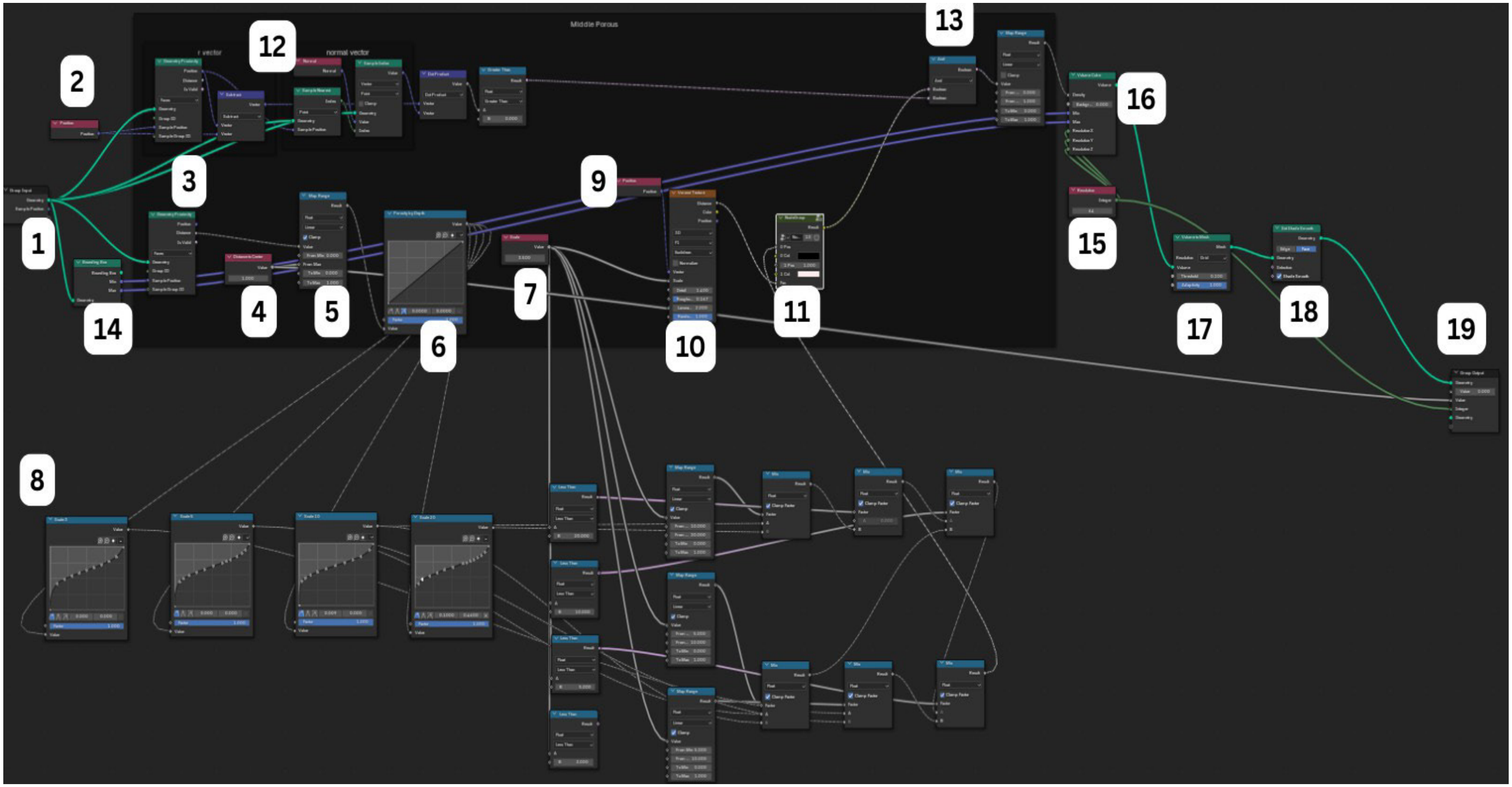

Figure 1. Diagram of the full node system (labeled items are detailed in Section 2.2.1).

Voronoi textures (Figure 2), cell-like distributions of polygonal shapes, generate Worley noise points. This process segments the item into voxels, then one point is distributed randomly in each voxel. These points create Voronoi cells from the set of points that are closer to a given point than any other generated point, which can have colormap criteria applied for adding multidimensional textures to solid objects. The radii of the voxels are determined by the scale node, which changes the spacing of the original points. The smaller the scale is, the larger the pore will be and vice versa.[10]

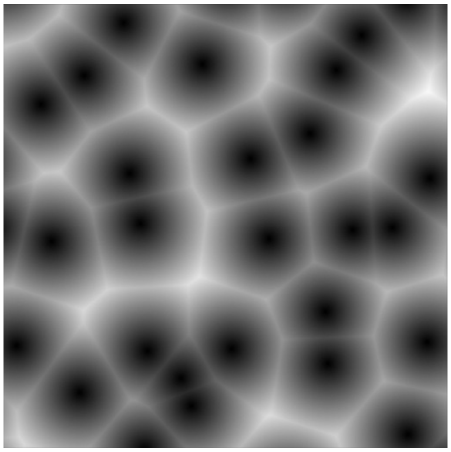

Figure 2. Sample of Voronoi texture from the Blender documentation.[10]

2.2.1 Geometry Nodes Step by Step

The guide below explains all the steps performed by the geometry nodes block by block, with each node or node group labeled in Figure 1 (nos. 1–19).

1) The "Group Input" node reads and outputs the geometry data of the imported model (Figure 3).

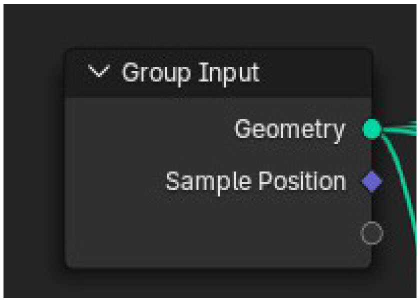

Figure 3. Group input node (no. 1 in Figure 1).

2) The "Position Output" node outputs the position of every point of the .stl vertices within the 3-D model (Figure 4).

Figure 4. Position output node (no. 2 in Figure 1).

3) Using the geometry from the group input node (see Figure 3), the block uses a "Geometry Proximity" node (Figure 5) to find how far every part of the geometry is from the nearest face, which will later be used to determine how porous that point should be.

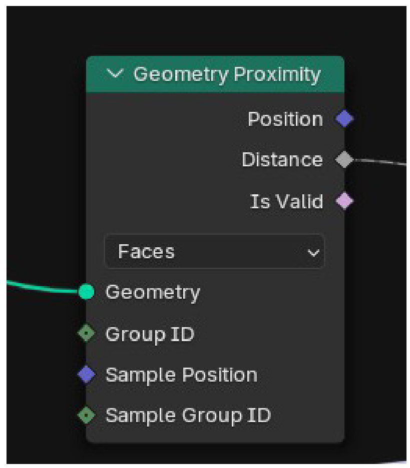

Figure 5. Geometry proximity node (no. 3 in Figure 1).

4) A "Value" node is used to specify the distance of the farthest inward point from the nearest face in the 3-D model (Figure 6). For example, in a cube, half the length of the sides would be entered, and in a sphere, it would be its radius. This can be based on a geometry that encompasses the desired model, e.g., a sphere that would surround a skull.

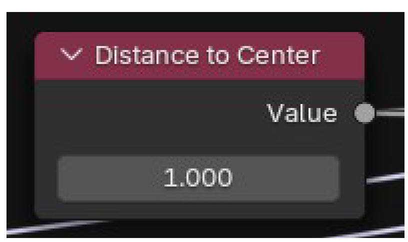

Figure 6. Value node (no. 4 in Figure 1).

5) The "Map Range" node (Figure 7) normalizes our distances for every point from 0 to 1 using the distance to the center we just entered (see Figure 6). This prepares the values to be inputs for a "Float Curve."

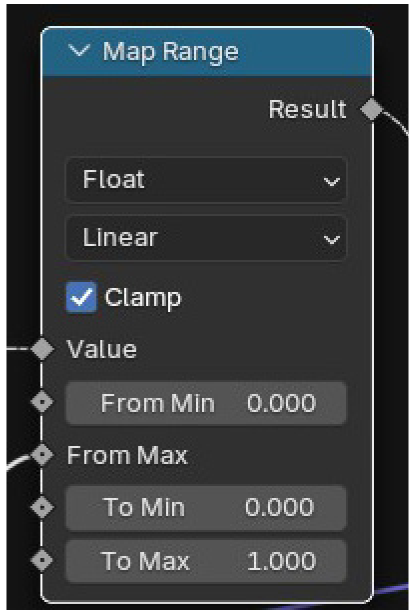

Figure 7. Map range node (no. 5 in Figure 1).

6) The "Float Curve" node allows the user to tell the algorithm what percentage porosity they want at every depth (Figure 8). For example, this float curve shows an object with a completely solid shell that is about 15% of the object and then becomes 75% porous on the inside.

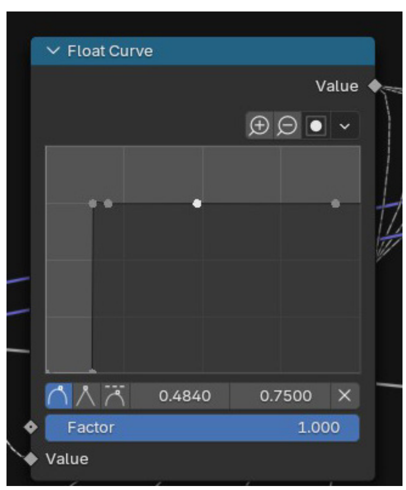

Figure 8. Float curve node (no. 6 in Figure 1).

7) Here we have another “Value” input node (Figure 9) where we put the scale for our Voronoi noise. A smaller scale means the texture will have bigger pores, and a bigger scale means smaller pores. The 3.5 scale produces an approximately 2-mm Voronoi cell. Scaling beyond 10 or below 1 tends to cause model or calculation time problems. The images show a 10-mm cube; the left image is at a 1.0 scale and the right is at 10.0

a)

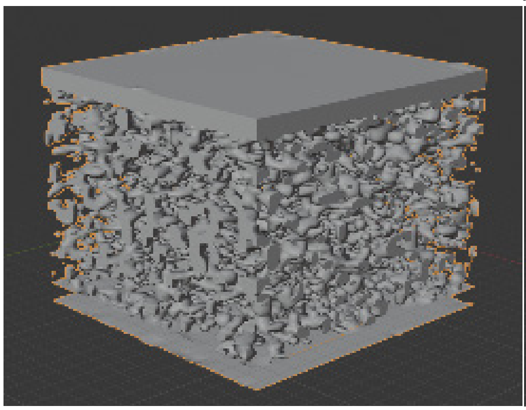

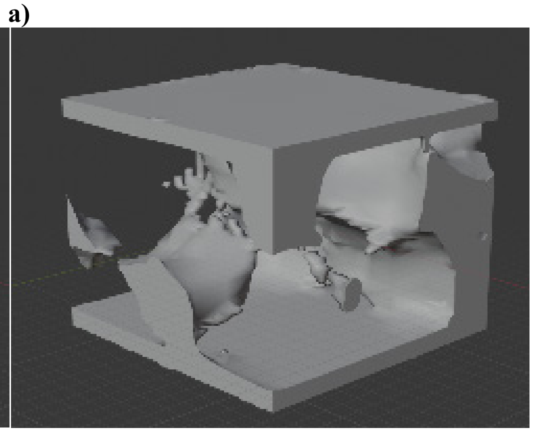

b) **c)**

Figure 9. a) Value input node with scale for Voronoi noise (no. 7 in Figure 1) with b) 10-mm cube at a 1.0 scale, and c) at 10.0.

8) This geometry node system (Figure 10) corrects for the error induced by scale selection—each segment is explained below.

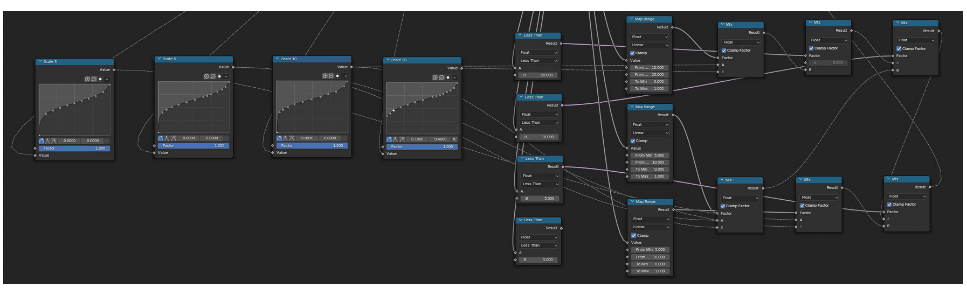

Figure 10. Geometry node system corrects for scale selection error (no. 8 in Figure 1).

a) The four Float Curve nodes (Figure 11) are empirically derived graphs that correct the error induced in the “Custom Color Ramp,” which is propagated into the final porosity. Each of these curves is calibrated at discrete Voronoi scales and are interpolated to transform inputs for scales among them.

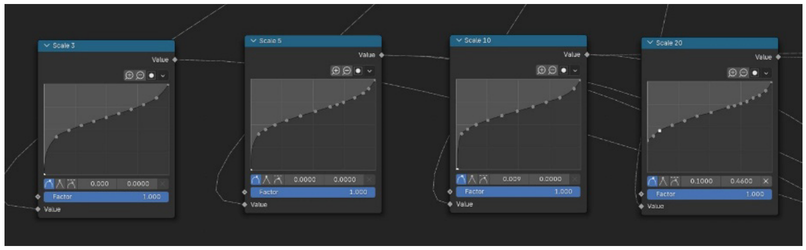

Figure 11. Float curve nodes (no. 8 in Figure 1).

b) On the other side, the scale is put through a collection of "Less Than" nodes (Figure 12) to determine which Float Curves will be used to scale the input.

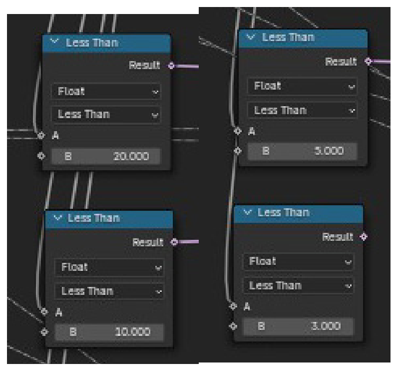

Figure 12. Less than nodes.

c) Finally, we use "Map Range" nodes (Figure 13), which normalize the scale input from the calibrated scale graphs to 0 to 1. These are interpolated by "Mix" nodes for the final output transform.

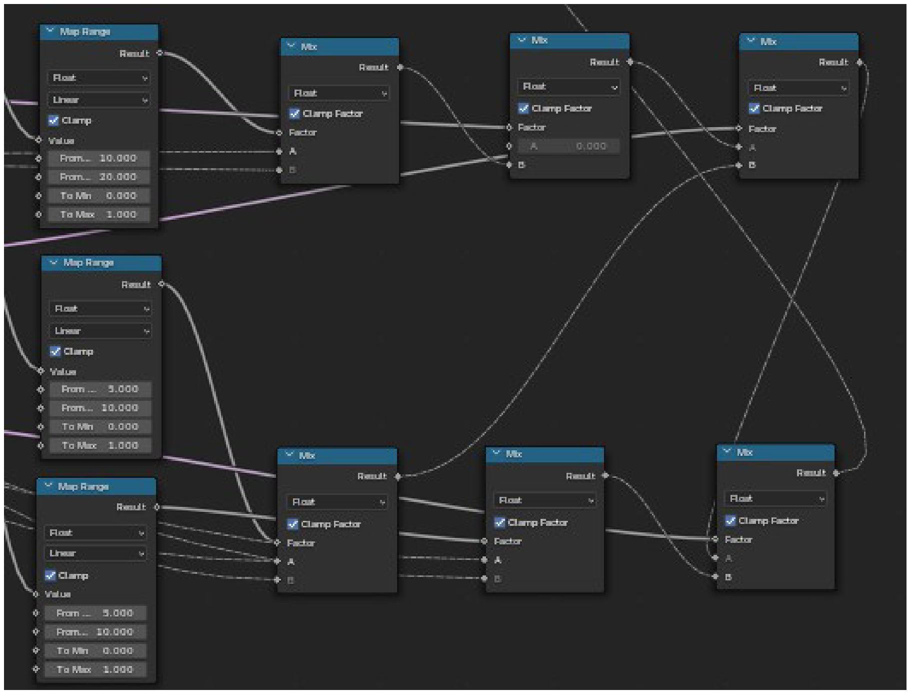

Figure 13. Map range nodes.

9) This "Position" node (Figure 14) exports the data of the Voronoi texture.

Figure 14. Position node (no. 9 in Figure 1).

10) This is the "Voronoi Texture" node (Figure 15) that generates the Voronoi noise based on the scale and position inputs. It exports the distance to the nearest Voronoi point. See Blender documentation for full discussion on this node's operation.[10]

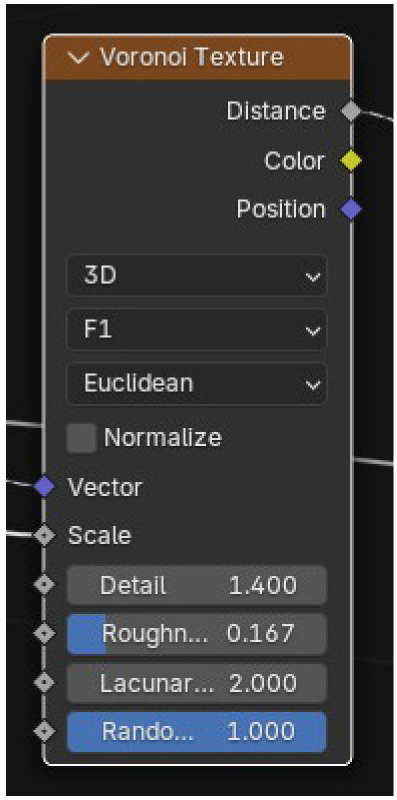

Figure 15. Voronoi texture node (no. 10 in Figure 1).

11) The "Custom Color Ramp" (Figure 16) takes the distance values from the Voronoi Texture node and the error correction from no. 8 (in Figure 1) to apply a color gradient to our model. We chose to break the standard node into its components for more precise control in our design.

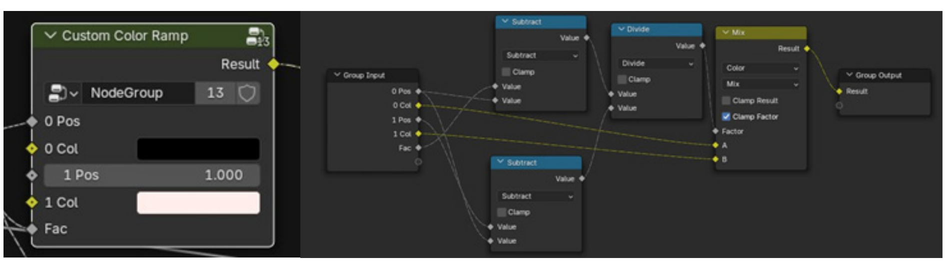

Figure 16. Custom color ramp (no. 11 in Figure 1).

12) Here, we take the position information from no. 2 (in Figure 1) and use it to generate an *r* vector to the surface using a "Geometry Proximity" node and "Subtract" node, then we create a normal vector to the surface by using a "Normal" node. The "Sample Nearest" node finds the nearest surface point from the chosen point; the "Sample Index" does this for each point in our geometry. Once we have both vectors, we use a "Dot Product" and a "Greater Than" to determine whether a point is in or outside the mesh.

Points found to be within the mesh are retained. This was drawn from a tutorial found at Ryo Mizuta Graphics.[11]

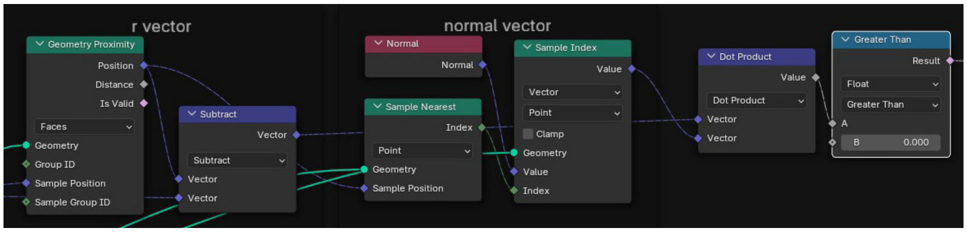

Figure 17. *r* and normal vectors (no. 12 in Figure 1).

13) This "And" node takes the outputs from nos. 12 and 8 (in Figure 1), so that only points within the bounds of the original mesh and points dictated by the Voronoi noise are rendered.

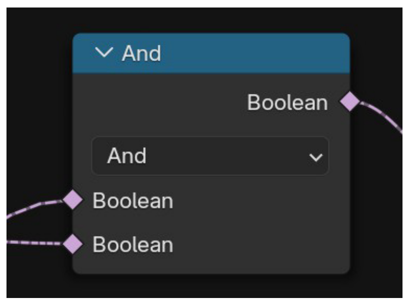

Figure 18. And node (no. 13 in Figure 1).

14) Here we have a "Bounding Box" (Figure 19) generated from our no. 14 (in Figure 1) geometry.

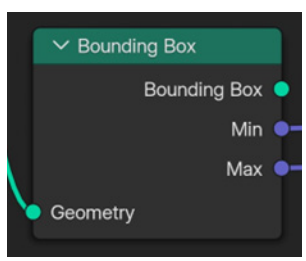

Figure 19. Bounding box (no. 14 in Figure 1).

15) This value node sets the "Resolution" for our final mesh (Figure 20). Higher resolution increases render time, but also model quality. The default value tends to cover most 3-D printable cases. Very small models require higher values, up to 128.

Figure 20. Value node for resolution (no. 15 in Figure 1).

16) Next, our "Volume Cube" node (Figure 21) takes the Resolution (no. 15 in Figure 1), the Bounding Box (no. 14), and the resultant map from no. 13. This maps the mathematical values we have been working with into a volume.

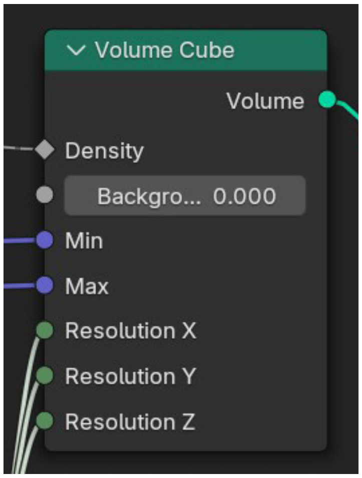

Figure 21. Volume cube node (no. 16 in Figure 1).

17) This "Volume to Mesh" node (Figure 22) generates a mesh along the surface of the volume.

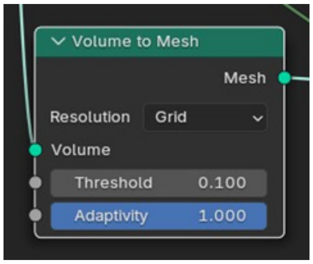

Figure 22. Volume to mesh node (no. 17 in Figure 1).

18) This "Set Shade Smooth" node (Figure 23) smooths any sharp edges that might result from the Voronoi generation.

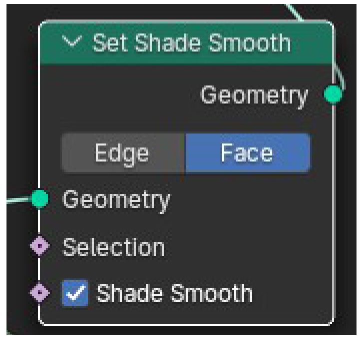

Figure 23. Set shade smooth node (no. 18 in Figure 1).

19) The final node is a "Group Output" node (Figure 24), which returns all the mesh data to the blender object to render.

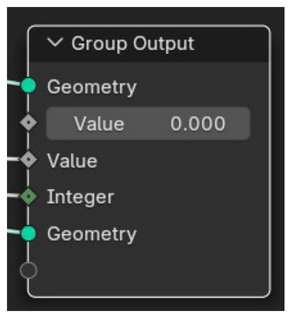

Figure 24. Group output node (no. 19 in Figure 1).

2.2.2 Method for Setting Desired Porosity

We implement two major nodes to alter the porosity: "Scale" and the "Porosity by Depth" graph. Pore size is inverse to the scale magnitude and only bound by the size of the object. The points on the "Porosity by Depth" graph can be moved to create a custom function; for example, this graph shows a porosity of 0% (solid) on the outside and linearly progresses to empty space at the center of the object. New points for finer control can be added or removed as necessary. These nodes are displayed in Figure 25.

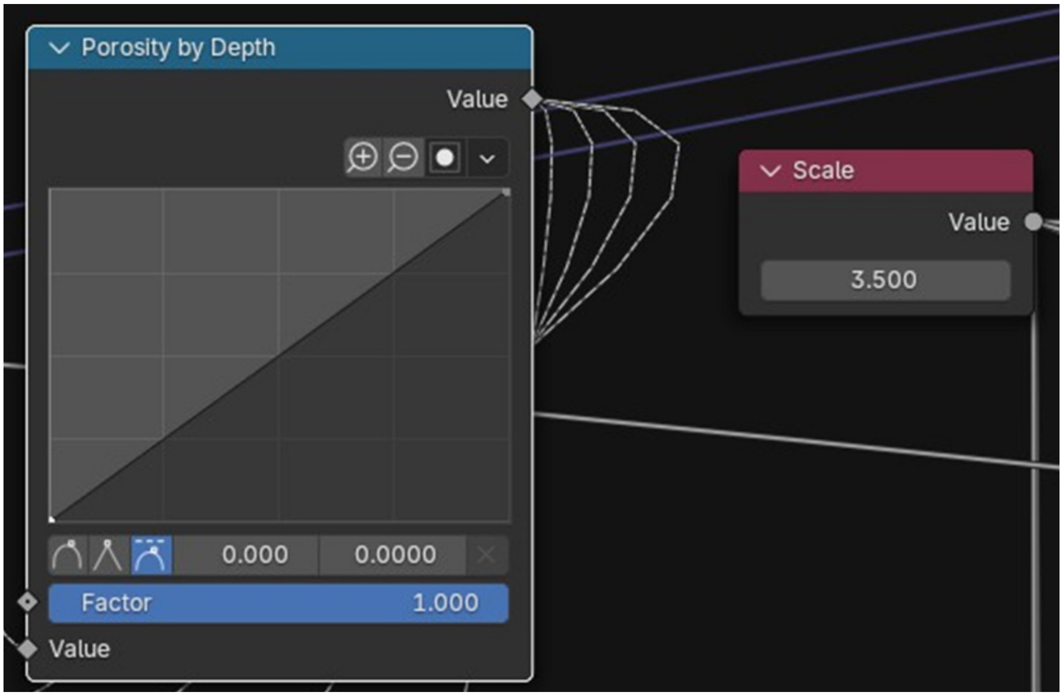

Figure 25. The two nodes used to change the porosity: scale and the porosity by depth.

2.3 Exporting from Blender and Printing the Cube

Materials used in the printing of porous structures include the following.

1) Formlabs Form 4 SLA printer (Formlabs Inc.; Somerville, Massachusetts)
   - Prints parts from resin using a Low Force Display print engine
2) Formlabs Wash L
   - Rinses parts to remove uncured resin
3) Formlabs Form Cure L
   - Applies consistent UV to finish curing printed parts
4) Formlabs PreForm 3.51.1.572
   - Software for preparing prints
5) Formlabs Clear V5 and Rigid 10K V1.1
   - Resins used: Technical Data Sheet available from Formlabs

We export the model as an .stl file from Blender and then import it to PreForm. We found that these patterns print best at roughly 45°—with the corner pointed down. Given the complexity of this geometry, this orientation minimizes the need for internal support and likelihood of failure, as displayed in Figure 26. Internal supports should be turned off, as they cannot be effectively removed from the complex internal structure. The smallest touchpoints tolerable should be used to allow for small external features to have support structure. Small local minima, displayed in red, will not print; however, this proves to be only 1%–3% of the structure. We chose commercial off-the-shelf resin—Formlabs Rigid 10K V1.1 and Clear V5 for printing—the former for its bone-like strength and the latter to visualize the interior structure. In each case, the smallest layer height feasible should be used to maximize structural detail.

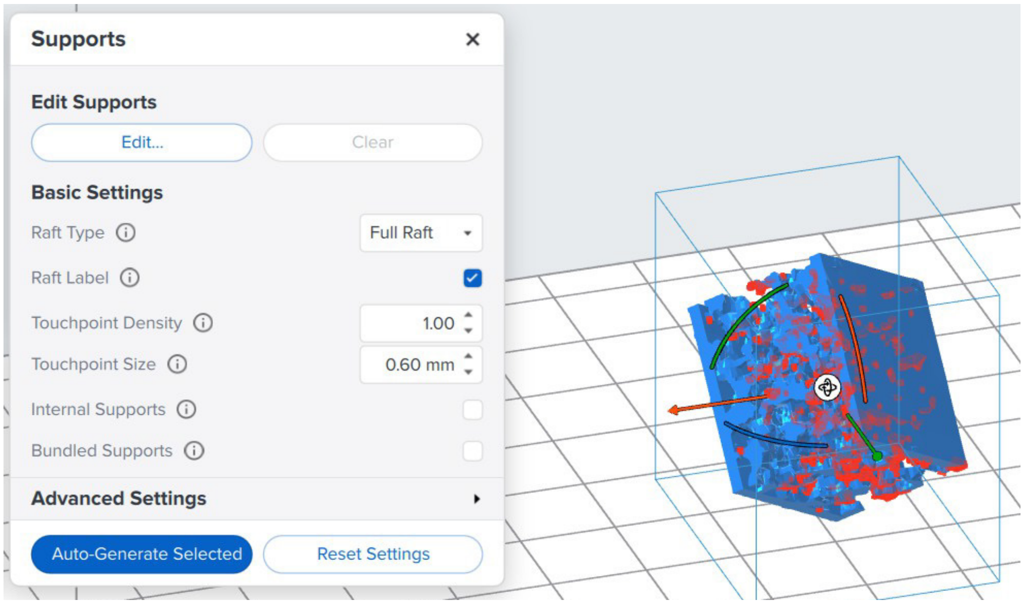

Figure 26. Support setting used and orientation of the test cube when printing.

2.4 Postprocessing Printed Samples

Resin prints require a solvent wash to remove uncured resin; these resins use isopropyl alcohol. Because of the small features, we elected to use two wash cycles, and at a 10-min duration per manufacturer's instructions. Each sample was allowed to dry completely before a second wash. Once fully dry, samples require a UV cure per manufacturer's instructions. This was completed in the Formlabs Cure L.

After curing we removed the printed support structure from the cubes and labeled each with a felt-tip pen on its porosity percentage, pore size, layer height, and alcohol wash number. We used flush-cut pliers and cut the supports at the surface from the model to protect any small features from accidental removal.

2.5 Mass and Porosity Calculation

Each sample's mass was recorded, and each was carefully inspected for uncured resin. We used Equation 1 to determine the porosity or empty volume fraction to compare to our expected porosity. This equation computes the difference in mass between a solid printed cube and our porous cubes, less the solid top and bottom.

$$Porosity = \left(1 - \frac{\text{Mass of the Sample} - \text{Mass of Solid Resin Cube} * \text{Volume fraction of solid surfaces}}{\text{Mass of Solid Resin Cube} * (1 - \text{Volume fraction of solid surfaces})}\right) * 100 \quad (1)$$

2.6 Infiltrating the Porous Bone Surrogate with Tissue Surrogate

To examine how well we could infiltrate these samples with tissue surrogates, we elected to test an agarose–glycerol–water hydrogel. A 3% weight/weight (w/w) Agarose RA (Avantor; Radnor, Pennsylvania) was microwave heated in a 30/70 w/w water/glycerol solution until fully clear. The cubes were placed in the solution in a vacuum oven (SVAC4, Sheldon Manufacturing; Cornelius, Oregon) at 80 °C and –14 inHg overnight. The cubes were then weighed and their mass was recorded. We compared the measured density of a gel cube of the same dimension of the test cube to the expected volume infill of each cube to compute actual infill percentage.

We first found that the gel had a density of 1.218 g/cm^3 and the Clear V5 resin has a density of 1.195 g/cm^3 by generating cubes of dimension 1 × 1 × 1.2 inches and taking the mass. Using this information, we were able to determine the amount the gel was able to infill the cube by comparing the expected to the actual mass of the finished cubes.

3. Results and Discussion

Figure 27 shows measured versus modeled bone volume fractions (BVFs). The black dots represent our best calibration curve used in Section 2.2.1.8. Yellow dots represent previous trials. Low BVFs tended to be more accurate than high BVFs. We postulate this is because higher BVFs prevent resin from escaping through narrow passages and small pores. This traps resin inside, which is unable to wash out. With this we calibrate our model to print accurately at an arbitrary BVF.

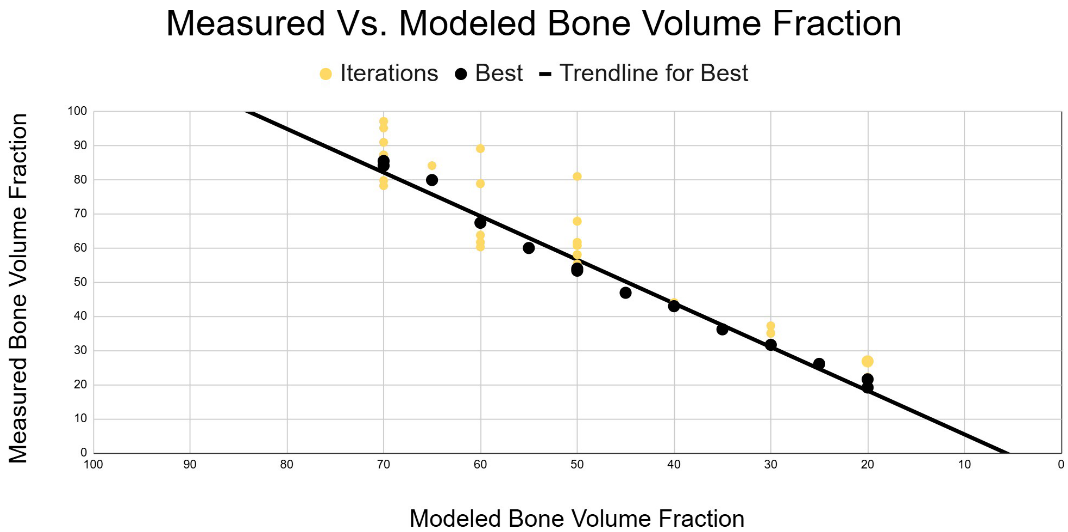

Figure 27. Modeled vs. measured BVFs.

Figure 28 shows the difference in print layer height and how it affects print accuracy. Figure 29 shows the Voronoi scale versus print accuracy, which is inversely correlated with pore size; 3.5 "Scale" produces approximately 2-mm pores, 10 is approximately 1 order of magnitude smaller. As expected, larger scale and larger print layers lead to less accurate prints. Some of these features approach the 30-µm limits of these printers, while other small gaps become unable to drain, completely isolated from the remaining structure, or erased with larger print layers. While extra wash cycles can help purge narrow spaces, too much exposure to such can negatively affect the structure. Large pores can create brittle models, so balance and calibration are necessary when designing a bone surrogate.

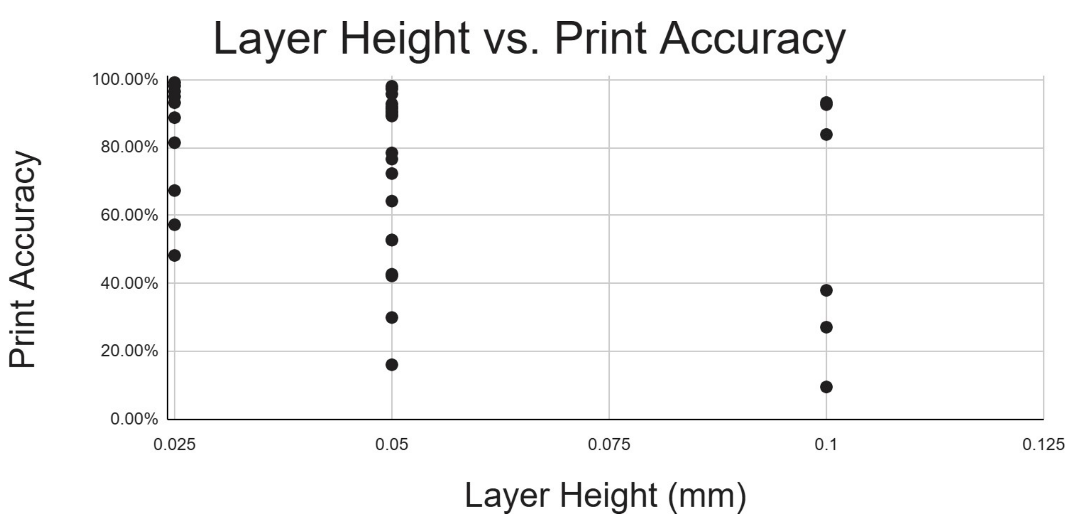

Figure 28. Scatter of set layer height vs. print accuracy.

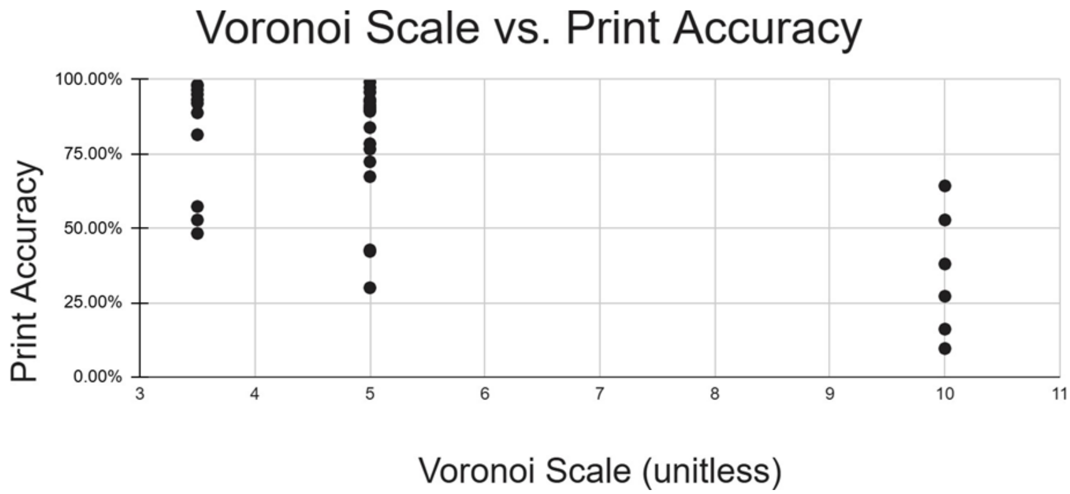

Figure 29. Scatter of Voronoi scale vs. print accuracy.

We chose three central porosities to infiltrate with hydrogel: 40%, 50%, and 60%. The 40% failed to fully infiltrate and was discarded. The 50% had a dry measured porosity of 46.305%. This sample partially infiltrated, with a 0.116% difference between expected and measured infiltrated mass. The 60% had a dry measured porosity of 56.71%. These larger pores allowed for a better infiltration, with only 0.03% difference between measured and expected mass.

4. Conclusion, Future Work, and Applications

We have taken micro-computed tomography scans to confirm our porosity calculations and are working on algorithmic confirmation of model accuracy and gel infill. With this confirmation, our next steps are to complete physical testing to match the physical properties of bone as seen in Alexander et al.[8] We then plan to examine how different gel infills can affect physical and EM properties of the overall tissue surrogate, with eventual goals of reproducing plates akin to skull. Overall, we have shown the first steps in producing biosimilar porous bone samples in arbitrary models and have determined the range in which we can accurately print our modeled porosity.

5. References

1. Plaisted TA, Gardner JM. Development of cranial bone surrogate structures using stereolithographic additive manufacturing. Army Research Laboratory (US); 2017 Sep. Report No.: ARL-TR-8163. https://apps.dtic.mil/sti/html/tr/AD1040863/

2. Hollensteiner M et al. Novel bone surrogates for cranial surgery training. J Mech Behav Biomed Mat. 2017;72:49–51. https://doi.org/10.1016/j.jmbbm.2017.04.021

3. Snapper DM et al. Development of a novel bioengineered 3D brain-like tissue for studying primary blast-induced traumatic brain injury. J Neurosci Res 2023;101(1):3–19. https://doi.org/10.1002/jnr.25123

4. Daru RR et al. Electrically equivalent head tissue materials for electroencephalogram study on head surrogates. Appl Sci. 2024;14(6):2495. https://doi.org/10.3390/app14062495

5. Kosterich JD, Foster KR, Pollack SR. Dielectric permittivity and electrical conductivity of fluid saturated bone. IEEE Trans Biomed Eng. 1983;30(2):81–86. https://doi.org/10.1109/tbme.1983.325201

6. Lee JHC et al. An investigation on the correlation between the mechanical properties of human skull bone, its geometry, microarchitectural properties, and water content. J Healthc Eng. 2019;2019:1–8. https://doi.org/10.1155/2019/6515797

7. Hoekema R et al. Measurement of the conductivity of skull, temporarily removed during epilepsy surgery. Brain Topogr. 2003;16(1):29–38. p. 10. https://doi.org/10.1023/a:1025606415858

8. Alexander SL, Rafaels K, Gunnarsson CA, Weerasooriya T. Structural analysis of the frontal and parietal bones of the human skull. J Mech Behav Biomed Mater. 2019;90:689–701. https://doi.org/10.1016/j.jmbbm.2018.10.035

9. Blender. Blender.org. Blender; n.d. [accessed 2026 Jan 8]. https://download.blender.org/source/

10. Blender Foundation. Blender 4.5 LTS manual; n. d. [last updated 2026 Jan 8]. https://docs.blender.org/manual/en/4.5/compositing/types/texture/voronoi.html

11. Ryo Mizuta Graphics. 3D graphics in scientific visualization. Ryo Mizuta Graphics; 2026 [accessed 2026 Jan 8]. https://ryomizuta.com

List of Symbols, Abbreviations, and Acronyms

3-D	Three-Dimensional
BVF	Bone Model Volume Fraction
EM	Electromagnetic
SLA	Stereolithography
.stl	Stereolithography (File)
UV	Ultraviolet
w/w	Weight/Weight

1 (PDF)	DEFENSE TECHNICAL INFORMATION CTR DTIC OCA
1 (PDF)	DEVCOM ARL FCDD RLB CI TECH LIB